Nanoscale

ROYAL SOCIETY OF CHEMISTRY

REVIEW

Cite this: *Nanoscale*, 2020, **12**, 15560

All-inorganic copper(I)-based ternary metal halides: promising materials toward optoelectronics

Zhihang Guo,[a,b,c] Junzi Li,[c] Ruikun Pan,*[a] Jiaji Cheng,[a,c] Rui Chen *[b] and Tingchao He *[c]

Received 2nd June 2020,
Accepted 30th June 2020

DOI: 10.1039/d0nr04220j

rsc.li/nanoscale

All-inorganic lead halides, including $CsPbX_3$ (X = Cl, Br, I), have become important candidate materials in the field of optoelectronics. However, the inherent toxicity of metal lead and poor material stability have hindered further applications of traditional metal halides, $CsPbX_3$. Therefore, copper(I)-based ternary metal halides are expected to become promising substitutes for traditional metal halides because of their nontoxicity, excellent optical properties and good stability under ambient conditions. This article reviews the recent development of all-inorganic low-dimensional copper(I)-based ternary metal halides by introducing their various synthesis methods, crystal structures, properties and their optoelectronic applications. In addition, the prospects for future challenges and the potential significance of copper(I)-based ternary metal halides in optoelectronic fields are presented.

1. Introduction

First discovered in 2014, all-inorganic lead halides, including $CsPbX_3$ (X = Cl, Br, I), have been widely recognized as a promising class of semiconductor materials for next-generation optoelectronics, owing to their high photoluminescence quantum yield (PLQY), tunable emission, and high absorption coefficient.[1–5] Considering these merits, great effort has been devoted to synthesizing various lead halides, investigating their photophysical properties, and developing their diverse applications such as solar cells,[6–9] light-emitting devices (LEDs),[10–14] photodetectors,[15,16] and lasers.[17,18] Despite considerable progress being made in the fabrication of lead halides, the toxicity of the metal lead and the poor stability of the materials limit their further applications. Under such circumstances, a strategy has been developed to replace toxic

[a]*Key Laboratory of Green Preparation and Application for Functional Materials, Ministry of Education, School of Materials Science and Engineering, Hubei University, Wuhan 430062, China. E-mail: rkpan@hubu.edu.cn*
[b]*Department of Electrical and Electronic Engineering, Southern University of Science and Technology, Shenzhen 518055, China. E-mail: chenr@sustech.edu.cn*
[c]*College of Physics and Optoelectronic Engineering, Shenzhen University, Shenzhen 518060, China. E-mail: tche@szu.edu.cn*

Zhihang Guo

Zhihang Guo received his BE degree from Hubei University in 2018. He is pursuing his MS degree under the supervision of Prof. Ruikun Pan at Hubei University. Currently, he is a visiting student at the College of Physics and Optoelectronic Engineering, Shenzhen University, China. His research interests include the synthesis and optical properties of semiconductor materials.

Junzi Li

Junzi Li is currently working toward her PhD at the SZU-NUS Collaborative Innovation Center for Optoelectronic Science & Technology, International Collaborative Laboratory of 2D Materials for Optoelectronics Science and Technology of Ministry of Education, College of Physics and Optoelectronic Engineering, Shenzhen University, China. Her current research interests concentrate on the optical properties of semiconductor nanomaterials and their applications.

lead with non-toxic ions such as tin, germanium and bismuth.[19–25] However, it was found that Sn^{2+} is easily oxidized to Sn^{4+} under ambient conditions due to its low chemical stability. Similarly, Ge- or Bi-based metal halides exhibit low emission efficiency, which still hampers their further optoelectronic applications.

According to the spatial arrangement of octahedral metal halide units, the crystal structure of metal halides can be divided into three-dimensional (3D) networks, two-dimensional (2D) layers, one-dimensional (1D) chains and zero-dimensional (0D) isolation structures at the molecular level.[26–28] Compared with 3D and 2D structures, low-dimensional metal halides exhibit unique photophysical properties due to their stronger quantum confinement effect (*cf.* 3D $CsPbBr_3$: exciton binding energy 19–62 meV, 0D Cs_4PbBr_6: 353 ± 40 meV).[29–32] The corner-connected $[PbX_6]^{4-}$ octahedral 3D networks enable excitons to dissociate easily owing to their low exciton binding energy.[29,33] Reduction in the molecular level dimension is conducive to improving the photophysical properties and thermal stability of low-dimensional materials,[34–36] which render them to be promising in various optoelectronic applications.[37–39] Hence, it is imperative to develop all-inorganic low-dimensional lead-free metal halides with excellent performance. Since Jun *et al.*[40] first reported the synthesis of 0D $Cs_3Cu_2I_5$ single crystals with a high PLQY of 90% and air-stability, low-dimensional Cu(I)-based ternary metal halides have attracted great attention due to their excellent photophysical properties and good stability. More importantly, to the best of our knowledge, there is no review article about Cu(I)-based metal halide materials at present. Therefore, we have summarized a detailed overview of the current progress made in the field of Cu(I)-based halides by concentrating on the following topics: (i) the reported fabrication strategies of all-inorganic Cu(I)-based ternary metal halides, (ii) their crystal structures, (iii) optoelectronic properties and stability, and (iv) related optoelectronic applications including LEDs, photodetectors, image sensors, fluorescent inks, and memristors. At the end of this review, we discuss the challenges of all-inorganic Cu(I)-based metal halides with a perspective of this research area on future directions.

2. Synthesis of copper(I)-based ternary metal halides

Over the past two years, many synthetic strategies have been developed to prepare copper(I)-based ternary metal halides and are introduced in the following sections, namely a hot injection route, crystal growth methods, a spin-coating approach and a solid-state reaction technique. In addition, various synthesis conditions and material sizes are also summarized in Table 1.

2.1 A hot-injection route

In 2014, Kovalenko's group pioneered to prepare all-inorganic cesium lead halides ($CsPbX_3$, X = Cl, Br, I and mixed halide systems) based on the hot-injection procedure.[5] Generally, under anhydrous and anaerobic conditions, cesium oleate is quickly injected into a 1-octadecene solution containing PbX_2, oleic acid and oleylamine at high temperature to form $CsPbX_3$ nanocrystals (NCs). Among them, oleic acid and oleylamine are used as cosolvents to change the kinetic process of the reaction, and on the other hand as surface ligands to passivate the NCs. Currently, as the most widely adopted procedure for the fabrication of $CsPbX_3$ NCs, the researchers further extended this approach to the synthesis of all-inorganic Cu(I)-based metal halides, as depicted in Fig. 1a. Cheng *et al.*[41] showed the colloidal synthesis of all-inorganic low-dimensional cesium copper halide NCs and demonstrated that reaction temperature is decisive for the final products. At a high reaction temperature (*ca.* 110 °C), the final products can be indexed as yellow-emitting $CsCu_2I_3$ NCs, while blue-emitting $Cs_3Cu_2I_5$ NCs are the final products at low temperature (*ca.* 70 °C). Almost simultaneously, Vashishtha *et al.*[42] described

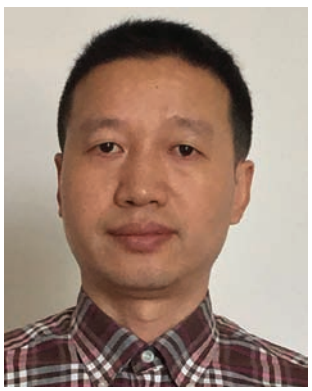

Ruikun Pan

Ruikun Pan received his PhD degree in Materials Science from Wuhan University of Science and Technology. He is currently working at School of Materials Science and Engineering at Hubei University. His research interests include optical properties of semiconductor materials and properties of ferroelectric materials.

Jiaji Cheng

Jiaji Cheng received his PhD degree from Université de Bordeaux in 2015. Afterwards, he went to Institut de Chimie de la Matière Condensée de Bordeaux (ICMCB) as a postdoc researcher in 2016. Then, he joined the School of Materials Science and Engineering, Hubei University as an associate professor. Currently, he is a visiting researcher at the College of Physics and Optoelectronic Engineering, Shenzhen University, China. His research interests involve nanophotonics, chiral plasmonics, and asymmetric synthesis.

Table 1 Summary of various synthetic approaches of Cu(I)-based ternary metal halides

Methods	Reactants	Reacting temperature	Size	Material	Ref.
Hot-injection route	Cs_2CO_3, CuX (X = I, Br, Cl), oleic acid and oleylamine (stabilizer), 1-octadecene (solvent)	70 °C	20 ± 2.5 nm	$Cs_3Cu_2I_5$ NCs	41
		110 °C	>1 μm	$CsCu_2I_3$ NCs	41
			≈43 nm	$Cs_3Cu_2I_5$ NPs	42
		150 °C	0.06 μm	$Cs_3Cu_2I_5$	43
			0.5–1 μm	$Cs_3Cu_2Cl_5$	46
		160 °C	≈68 × 201 nm^2	$CsCu_2I_3$ NRs	42
			17.5 nm	$Cs_3Cu_2I_5$ NCs	45
		180 °C	≈1 μm	$Cs_3Cu_2Cl_5$	43
			≈0.99 × 0.22 μm^2	$Cs_3Cu_2Br_5$	43
	Add InX_3 (X = I, Br, Cl)	180 °C	30 × 20 × 10 nm^3	$Cs_3Cu_2I_5$ NCs	79
			21–28 nm	$Cs_3Cu_2Cl_5$ NCs	79
		200 °C	12–15 nm	$Cs_3Cu_2Br_5$ NCs	79
	Replace CuX with $Cu(OAc)_2$, I_2 and HX acid (X = Br, Cl)	120 °C	21 × 14 nm^2	$Cs_3Cu_2I_5$ NCs	44
			21 × 11 nm^2	$Cs_3Cu_2Br_5$ NCs	44
			13 nm	$Cs_3Cu_2Cl_5$ NCs	44
Antisolvent vapor-assisted crystallization	CsI, CuI, DMF and DMSO (solvent), MeOH (antisolvent)	60 °C	≈5 mm	$Cs_3Cu_2I_5$ SCs	40
			10 × 1.5 mm^2	$CsCu_2I_3$ SCs	48
Rapid antisolvent crystallization	CsI, CuI, GBL (solvent), and isopropanol (antisolvent)	RT	N.A.	$Cs_3Cu_2I_5$ and $CsCu_2I_3$	50
	CsI, CuI, acetonitrile (solvent), and ether (antisolvent)		35 nm–6.0 μm	$CsCu_2I_3$ NWs	49
Inverse temperature crystallization	CsI, CuI, DMF (solvent), and toluene (titrant)	100 °C	≈2 mm	$CsCu_2I_3$ SCs	52
Temperature-lowering crystallization	RbX, CuX, HX acid (X = Cl, Br) (solvent), and hypophosphorus acid (antioxidant)	95 °C	N.A.	Rb_2CuCl_3 SCs	55
		135 °C	≈3 cm	Rb_2CuCl_3 SCs	56
		100 °C	≈200 μm	Rb_2CuBr_3 SCs	57
	CsI, CuI, HI acid (solvent), and hypophosphorus acid (antioxidant)	80 °C	N.A.	$CsCu_2I_3$ SCs	54
Solvent evaporation crystallization	CsI, CuI, and DMF (solvent)	RT	1–5 mm	$CsCu_2I_3$	59
Solid-state reaction technique	RbX and CuX (X = Cl, Br)	225 °C	N.A.	Rb_2CuX_3	55
	CsX and CuX (X = I, Br, Cl)	RT	N.A.	$Cs_3Cu_2X_5$ and $CsCu_2X_3$	62
		410 °C	N.A.	$CsCu_2X_3$	69
	CsI, CuI and $MnCl_2$	450 °C	N.A.	Mn doped $Cs_3Cu_2I_5$	70

the synthesis of $Cs_3Cu_2I_5$ nanoplates (NPs) and $CsCu_2I_3$ nanorods (NRs) with controlled shape and composition, and regulated their functions by adjusting the reaction temperature and ligand proportions.

Subsequently, several groups employed similar hot-injection routes to synthesize $Cs_3Cu_2X_5$ (X = Cl, Br, I) NCs with different optical properties and chemical compositions.[43–46] For instance, Luo *et al.*[44] investigated the photophysical pro-

Rui Chen

Rui Chen received his PhD degree in Applied Physics from Nanyang Technological University, and in Physics from Xiamen University. He is currently working at the Department of Electrical and Electronic Engineering at Southern University of Science and Technology. His research interests include laser spectroscopy, optical properties of materials, optical microcavity and micro/nano lasers.

Tingchao He

Tingchao He received his PhD degree in Optics from Shanghai Jiao Tong University in 2010. Afterwards, he went to Nanyang Technological University as a research fellow from 2010 to 2014. He is currently working at the College of Physics and Optoelectronic Engineering of Shenzhen University. His research interests include ultrafast spectroscopy and chiral optics of novel optoelectronic materials.

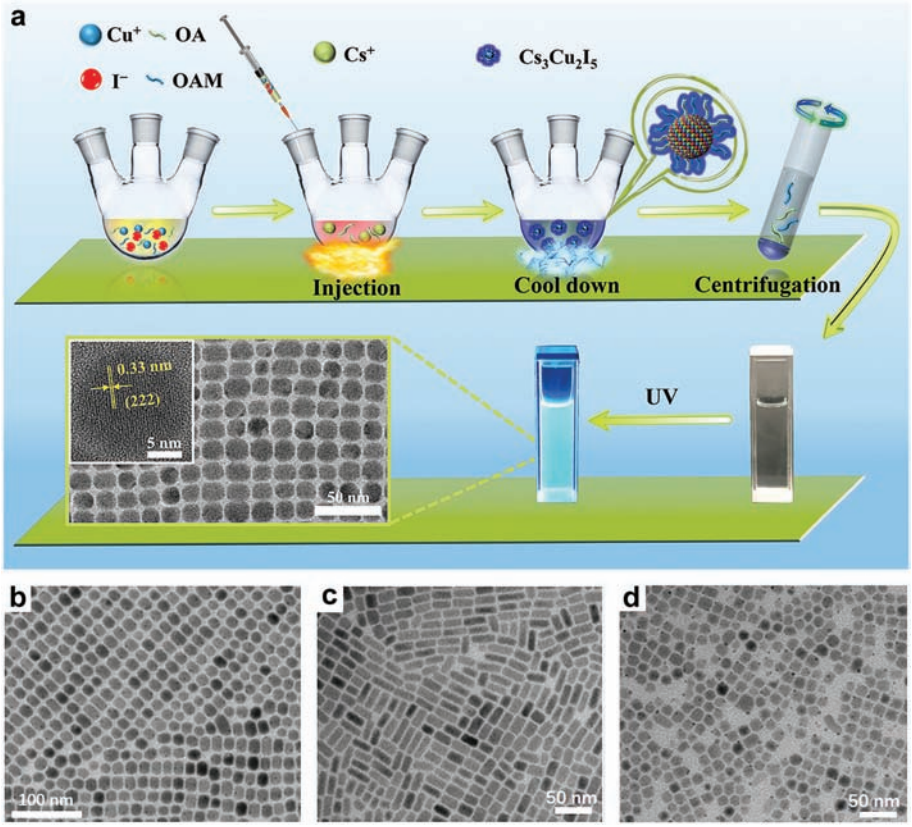

Fig. 1 Hot-injection route for the synthesis of Cu(I)-based metal halides. (a) Schematic diagram for the colloidal synthesis of $Cs_3Cu_2I_5$ NCs (top), photographs of $Cs_3Cu_2I_5$ NCs colloidal solution under ambient conditions and 254 nm excitation, and the corresponding TEM images (bottom). Reproduced with permission from ref. 45. Copyright 2020, American Chemical Society. Typical TEM images of (b) $Cs_3Cu_2I_5$, (c) $Cs_3Cu_2Br_5$ and (d) $Cs_3Cu_2Cl_5$ NCs. Reproduced with permission from ref. 44. Copyright 2020, Wiley-VCH.

perties and stability of the synthesized $Cs_3Cu_2X_5$ and found that $Cs_3Cu_2Cl_5$ NCs have the highest PLQY and exhibit excellent PL stability in air. The typical transmission electron microscopy (TEM) images of the as-prepared $Cs_3Cu_2X_5$ NCs are illustrated in Fig. 1b–d. Both $Cs_3Cu_2I_5$ and $Cs_3Cu_2Br_5$ NCs show a rod-like morphology, while $Cs_3Cu_2Cl_5$ NCs exhibit a cube-like shape. In addition, Lian *et al.*[43] synthesized a series of $Cs_3Cu_2X_5$ NCs. They demonstrated that the addition of ethyl acetate to the crude solution during the purification process was a key parameter to improve blue emission efficiency. Notably, the PL emission shows a gradual redshift with halogen, which is contrary to the general trend found in $CsPbX_3$ NCs. They illustrated that the abnormal PL spectra of $Cs_3Cu_2X_5$ are attributed to the synergetic combination of the significant change in the bandgap associated with structural deformation and large excitonic effect.

2.2 Crystal growth methods

2.2.1 Antisolvent vapor-assisted crystallization. The antisolvent vapor-assisted crystallization method is based on the different solubility behaviors of metal halide materials in different solvents to grow crystals.[47] In general, metal halides show high solubility in solvents such as *N*,*N*-dimethylformamide (DMF) and dimethyl sulfoxide (DMSO), and low solubility in toluene and chloroform. These solvents with low solubility for metal halides are called antisolvents. Typically, the slow diffusion of antisolvent vapor into the precursor solution (consisting of metal halides dissolved in good solvents) leads to solution supersaturation and initiates crystal formation and growth. Jun *et al.*[40] reported for the first time that lead-free 0D $Cs_3Cu_2I_5$ single crystals (SCs) with a size of about 5 mm were produced by this method. Inspired by this, Lin *et al.*[48] obtained other $CsCu_2I_3$ phase SCs, which were effectively controlled by easily changing the ratio of cesium iodide (CsI) and copper(I) iodide (CuI) in the precursor solution. Generally, heating the antisolvent can accelerate the growth of crystals. However, it takes relatively a longer time for single-crystal growth (*e.g.*, temperature: 60 °C, time: 48 h) and it is difficult to obtain large sized SCs.

2.2.2 Rapid antisolvent crystallization. Rapid antisolvent crystallization is another method of rapid synthesis of crystals evolved on the basis of the antisolvent vapor-assisted crystallization method. The reaction is usually carried out at room temperature and does not require a long time to grow crystals. Li's group synthesized high-quality, adjustable-size ternary copper-based halide $CsCu_2I_3$ nanowires (NWs) and applied

them to polarization-sensitive and flexible ultraviolet photodetectors.[49] Fang *et al.*[50] dissolved CsI and CuI in γ-butyrolactone (GBL) at a specific molar ratio to form the precursor solution, and then rapidly injected the precursor solution into the antisolvent isopropanol to obtain crystals (Fig. 2a). They successfully demonstrated that chemical conversion between $Cu_3Cu_2I_5$ and $CsCu_2I_3$ can be realized by a simple mechanical grinding method. To be specific, the conversion process can be described as the following two reactions: (i) $Cu_3Cu_2I_5 + 4CuI \rightarrow 3CsCu_2I_3$ and (ii) $CsCu_2I_3 + 2CsI \rightarrow Cu_3Cu_2I_5$, and the reaction mechanism is described as shown in Fig. 2b. They found that addition of water, ethanol or propanol during the grinding process can promote the abovementioned two reactions, but it is more difficult to achieve complete conversion for the second reaction.[50] Overall, choosing of appropriate precursors or additives for the mechanochemical reaction can further tune the emitting wavelength of Cu(I)-based metal halides, which may provide a new pathway for future applications of white LEDs.

2.2.3 Inverse temperature crystallization. Metal halides possess inverse temperature solubility behavior in some certain solvents with increasing temperature.[51] Based on this, the inverse temperature crystallization method can be implemented through heating of the precursor solution with an appropriate concentration. Jun's group manufactured 1D $CsCu_2I_3$ SCs with a size of ~2 mm through this method.[52] The CsI–CuI solution with a concentration of 0.25 M was prepared using DMF as a solvent, and the precursor solution after toluene titration and filtration treatment was then maintained at a temperature of 100 °C for 30 min to grow crystals. Importantly, such crystallization possesses a simple procedure and an order of magnitude faster crystallization rate compared to those previously reported classical growth approaches, which makes it a relatively common method for preparing metal halide crystals.[51]

2.2.4 Temperature-lowering crystallization. The temperature-lowering crystallization method is implemented based on the principle that the solubility of metal halides in an aqueous

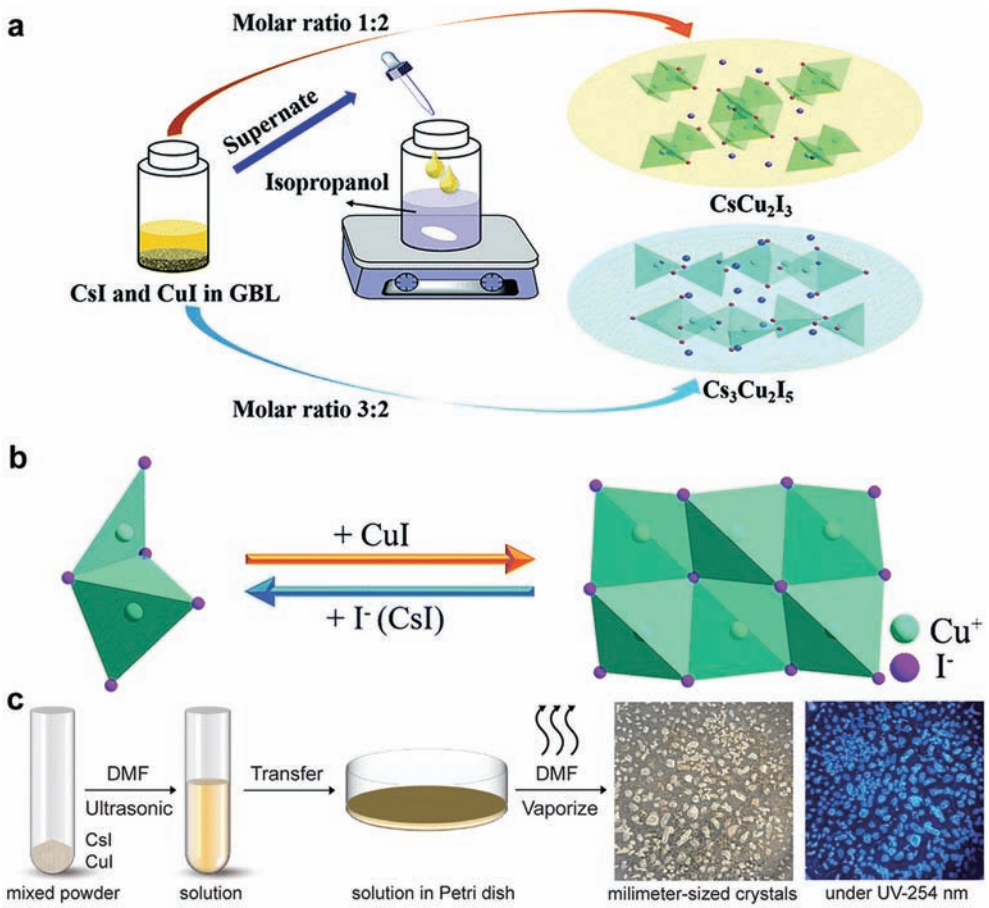

Fig. 2 Crystal growth methods for the synthesis of Cu(I)-based metal halides. Schematic illustration of (a) the synthetic process for cesium copper iodide with different stoichiometric ratios and (b) conversion between the 0D site of $[Cu_2I_5]^{3-}$ and the 1D structure of $[Cu_2I_3]^-$. Reproduced with permission from ref. 50. Copyright 2020, the Royal Society of Chemistry. (c) Schematic diagram of the room temperature solvent evaporation crystallization process to synthesize $Cs_3Cu_2I_5$ crystals, and the corresponding photographs under day light and the UV lamp. Reproduced with permission from ref. 59. Copyright 2020, Wiley-VCH.

solution of hydrohalic acid decreases with the decrease in solution temperature.[53] Typically, a saturated solution of metal halides is prepared at a higher temperature, and then the precursor solution is cooled to a certain level at a slow rate to supersaturate the solution and precipitate the crystals. Through this method, Li *et al.*[54] successfully synthesized 1D $CsCu_2I_3$ by slowly cooling the precursor solution (formed by dissolving CsI and CuI in hydroiodic acid at 100 °C) at a rate of 1 °C h^{-1}. In particular, the addition of hypophosphorus acid to the precursor solution avoids oxidation of Cu^+ during the heating procedure. Also, they investigated the pressure-induced enhancement of PL behavior in 1D $CsCu_2I_3$, which showed a new strategy for low-dimensional metal halide emission modulation. Furthermore, another low-dimensional Cu(I)-based metal halide Rb_2CuX_3 (X = Cl, Br) has also been reported by some researchers.[55–57] Among them, Creason's group pioneered to investigate the up-conversion PL behavior of lead-free metal halide Rb_2CuCl_3 and the optical cooling efficiency can be estimated to be about 32%. Hence, this method is a convenient and effective approach for crystal growth, and we look forward to extending it to the synthesis of other phases (*e.g.*, 0D $Cs_3Cu_2X_5$).

2.2.5 Solvent evaporation crystallization. Based on evaporation and concentration of the precursor solution to induce crystallization, the solvent evaporation crystallization method is a conventional and simple strategy to grow crystals.[58] Zhang *et al.*[59] ultrasonically dissolved CuI and CsI (molar ratio of 2 : 3) in DMF, and then placed the precursor solution under a fume hood to evaporate the solvent, resulting in the formation of $Cs_3Cu_2I_5$ crystals (Fig. 2c). The size of the obtained $Cs_3Cu_2I_5$ crystals can be adjusted by the concentration of the precursor in the DMF solution. Specifically, $Cs_3Cu_2I_5$ crystals with a size larger than 5 mm were obtained by evaporating high concentration (0.4 M) of the precursor solution, while the crystals with a size smaller than 1 mm were produced at low concentration (0.125 M). The solvent evaporation crystallization method can also be extended to fabricate yellow-emitting $CsCu_2I_3$ crystals by adjusting the molar ratio of CsI : CuI to 1 : 2.[59] Although this method is convenient and efficient to grow crystals, it is difficult to precisely control the growth of large crystals.

2.3 A spin-coating approach

The most typical method to prepare metal halide films is the one-step spin-coating technique, in which the resulting precursor solution is spin-coated on the substrate and is then thermally annealed to obtain thin films.[28] Typically, the precursor solution is obtained by dissolving metal halides (molar ratio of CsI : CuI: 3 : 2 for $Cs_3Cu_2I_5$ and 1 : 2 for $CsCu_2I_3$) sequentially into a mixed solvent of DMSO and DMF.[40,52,60–62] Besides, another modified one-step method called antisolvent engineering was developed to prepare dense and uniform halide films, which has been reported in traditional Pb-based halides.[63,64] Ma *et al.*[65] evaluated the influences of antisolvent dripping time on the morphology of $CsCu_2I_3$ films, in which appropriately prolonged dripping time helped to obtain a dense and uniform surface, but further increasing the dripping time would lead to morphology deterioration (Fig. 3). The $CsCu_2I_3$ films with better luminous performance can be obtained by precisely controlling the dripping time of the anti-

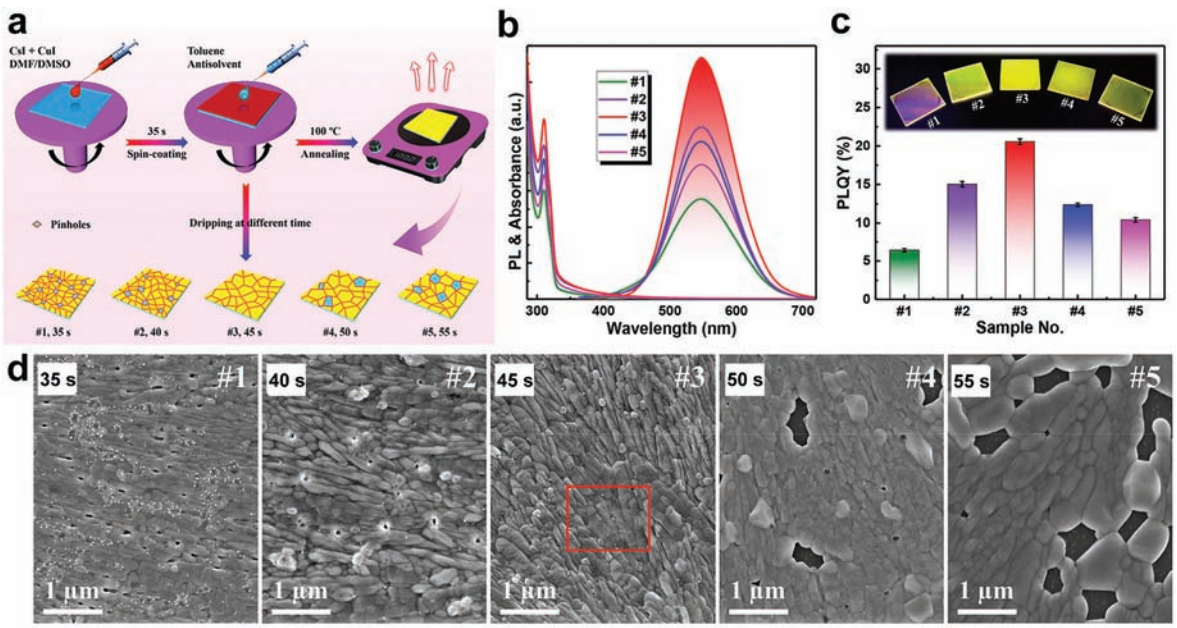

Fig. 3 Spin-coating approach for the synthesis of Cu(I)-based metal halides. (a) Schematic diagram of synthesis of $CsCu_2I_3$ thin films with different dripping time of toluene antisolvent. (b) Absorption, PL spectra and (c) PLQYs of the $CsCu_2I_3$ thin films. Insets: Photographs of the $CsCu_2I_3$ thin films under 254 nm excitation. (d) Scanning-electron microscopy images of the $CsCu_2I_3$ thin films. Reproduced with permission from ref. 65. Copyright 2020, American Chemical Society.

solvent. In a typical procedure, the antisolvent was quickly added dropwise onto the precursor-coated substrate to reduce the solubility of the precursor solution, thus promoting crystal nucleation and film formation.[66] Overall, as a universal method of preparing high quality dense and pinhole-free halide films, dripping antisolvent after spin coating is vital to precisely control the dripping time to adjust the film morphology.

2.4 The solid-state reaction technique

As a way of the solid-state reaction technique, mechanochemical synthesis has emerged as an attractive synthetic procedure with obvious simplicity, rapidity, reproducibility, and environment friendliness and possesses tremendous potential for the extension of the design of various metal halide structures.[67,68] In such green chemistry, Sebastia-Luna *et al.*[62] conveniently obtained $CsCu_2X_3$ and $Cs_3Cu_2X_5$ compounds by stoichiometric ball milling or grinding of CsX and CuX (X = Cl, Br, I or their mixture) at room temperature without dissolving them in solution. The composition of metal halides can be flexibly adjusted through various combinations of Cl, Br, and I contents, thereby actualizing emission modulation. In addition, high-temperature sintering of stoichiometric-grinding precursors is also designed to produce Cu(I)-based halides and Mn-doped halides.[69,70] A series of novel Mn-doped dual-emitting $Cs_3Cu_2I_5$ thermochromic halides were prepared by Du's group.[70] Under irradiation of 300 nm, these obtained microparticles not only exhibit the featured emission of Cu^+ but also a green emission at 556 nm from the $^4T_{1g} \rightarrow {}^6A_{1g}$ transition of Mn^{2+}. Induced by the thermal quenching effect, the emission intensities of both Cu^+ and Mn^{2+} decreased with increasing temperature, and Cu^+-related emission was more sensitive to the temperature compared with that of the Mn^{2+}, which was described as the origin of thermochromism.

3. Crystal structures

As early as 2004, Hull *et al.*[71] systematically studied crystal structures of ternary derivatives of copper monohalides. Fig. 4a–c show three typical schematic crystal structures of Cu(I)-based halides. To be specific, 0D $Cs_3Cu_2I_5$ crystallized in the *Pnma* space group of the orthorhombic crystal system, in which Cu^+I_4 tetrahedra and a Cu^+I_3 triangle that are edge-connected to form isolated $[Cu_2I_5]^{3-}$ units were separated by the surrounding Cs^+ ions. In contrast, 1D $CsCu_2I_3$ belongs to the orthorhombic space group of *CmCm*, where Cu^+I_4 tetrahedra share common edges thereby forming infinite double chains of composition of Cu_2I_3 interspersed by Cs^+ ions. Furthermore, Rb_2CuX_3 (X = Br and Cl) is crystallized in the orthorhombic space group *Pnma*, featuring 1D $[CuX_3]^{2-}$ chains separated by Rb^+ ions. Cu^+X_4 tetrahedra share a common corner thus forming $[CuX_3]^{2-}$ chains along the *b*-axis and resulting in a 1D structure. Sebastia-Luna's group demonstrated that a continuous shift in the Bragg's reflection peaks

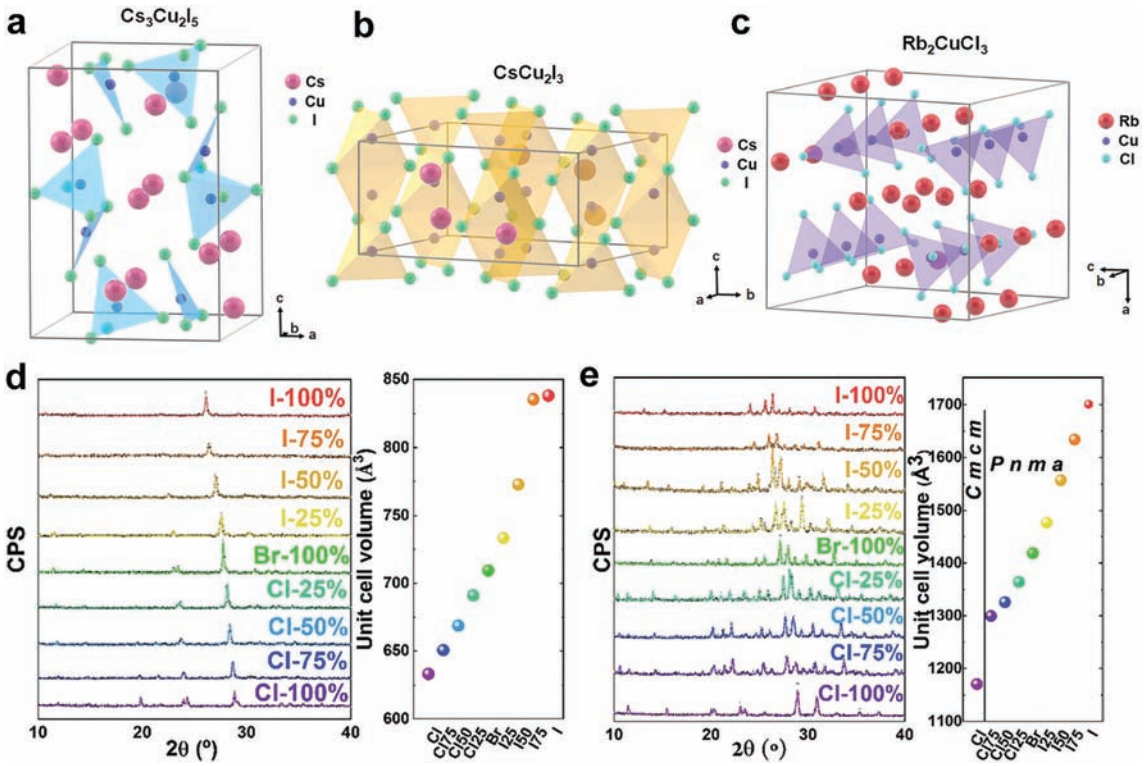

Fig. 4 Crystal Structures of Cu(I)-based metal halides (a) $Cs_3Cu_2I_5$, (b) $CsCu_2I_3$ and (c) Rb_2CuCl_3. X-ray diffraction patterns (left) and unit cell volume (right) of (d) $CsCu_2X_3$ and (e) $Cs_3Cu_2X_5$ compounds. Reproduced with permission from ref. 62. Copyright 2019, American Chemical Society.

is linearly dependent on the composition, indicating the formation of high phase purity compounds (Fig. 4d).[62] Exceptionally, Cl-rich mixed Br–Cl compounds reveal minor phase segregation between $CsCu_2Br_3$ and $CsCu_2Cl_3$ domains. In addition, unit cell volumes derived from Le Bail fits show a rather linear expansion from 633 Å^3 (X = Cl) to 710 Å^3 (X = Br) and 838 Å^3 (X = I), due to lattice expansion or contraction caused by the insertion of the larger I^- ion or the smaller Cl^- ion.[62] Similarly, for the crystal structures of $Cs_3Cu_2X_5$, diffractograms are fitted by the *Pnma* space group (Fig. 4e). In this work, they found that the Cl-rich compounds (75 and 100%) are better fitted by the space group *CmCm*, which may lead to distinguishable optical properties of Cl-rich compounds consistent with their different crystalline phases.[62] Obviously, the inability to clarify what drives the crystallization in this structure seems to hinder the understanding of the relationship between the lattice structure and the optical properties of the Cu(I)-based metal halides. Therefore, further experimental studies to elucidate the structural characteristics and mechanism of metal halides are essential for a better understanding of these materials.

4. Properties

4.1 Electronic structures

Most properties (such as charge transfer and optical properties) of metal halide systems are determined by their electronic structures, including the spatial and energy distribution of electrons. Up to now, a lot of comprehensive research work has been conducted on the band structures, density of states (DOS) and many other electronic properties of Cu(I)-based metal halides. The valence band (VB) is predominantly composed of the Cu 3d orbital hybridized with the halide *n*p orbitals (*n* is the principal quantum number, *n* = 3, 4, and 5 for Cl, Br, and I, respectively), while the conduction band (CB) is mainly contributed by admixed Cu 4s and the halide *n*p orbitals.[43,44,55] Cs^+ ions are far away from valence and conduction bands, so their contribution to the VB and CB is too small to be considered.[40,48] Fig. 5 shows the typical electronic structures and projected DOS of Cu(I)-based halides, in which the colloidal 0D $Cs_3Cu_2I_5$ and 1D $CsCu_2I_3$ NCs are calculated to possess direct band gaps from density functional theory (DFT).[41] It was notable that the highest valence band of $Cs_3Cu_2I_5$ is flatter than that of $CsCu_2I_3$, symbolizing heavier electron and hole effective masses and strong quantum confinement, thereby resulting in a strong emission.[46,52]

In addition, the electronic structure of Cu(I)-based halides will change significantly upon photoexcitation, which is closely linked to their optical properties. Fig. 6a–c reflect the projected DOS of $Cs_3Cu_2X_5$ before and after photoexcitation, and additional peaks were observed above the valence band (VB) in the photoexcited state when compared to the pristine structure, indicating stronger coupling in the low-dimensional structure.[43] Such charge localization can be attributed to the obvious structural deformation that occurs when the $[Cu_2X_5]^{3-}$ cluster transitions from the ground state to the excited state. As a result, the length of the Cu_1–Cu_2 bond decreases from 2.53 to 2.33 Å, while the Cl–Cu_1–Cu_2 angle increases from 147° to 177°.[43] The phenomenon of lattice structure deformation of Cu(I)-based halides upon photoexcitation is consistent with that reported in ref. 45, as illustrated in Fig. 6d. Similarly, the excitons of 1D $CsCu_2I_3$ tend to localize due to the large structural distortion of $[Cu_2I_6]^{4-}$ tetrahedra upon photoexcitation. Specifically, I_1 and I_3 will stretch in opposite directions, while Cu_1 and Cu_2 will shrink toward the center (Fig. 6e).[65] Besides, due to the lattice deformation of metal halide structures, the broad band PL emission with a large Stokes shift is usually

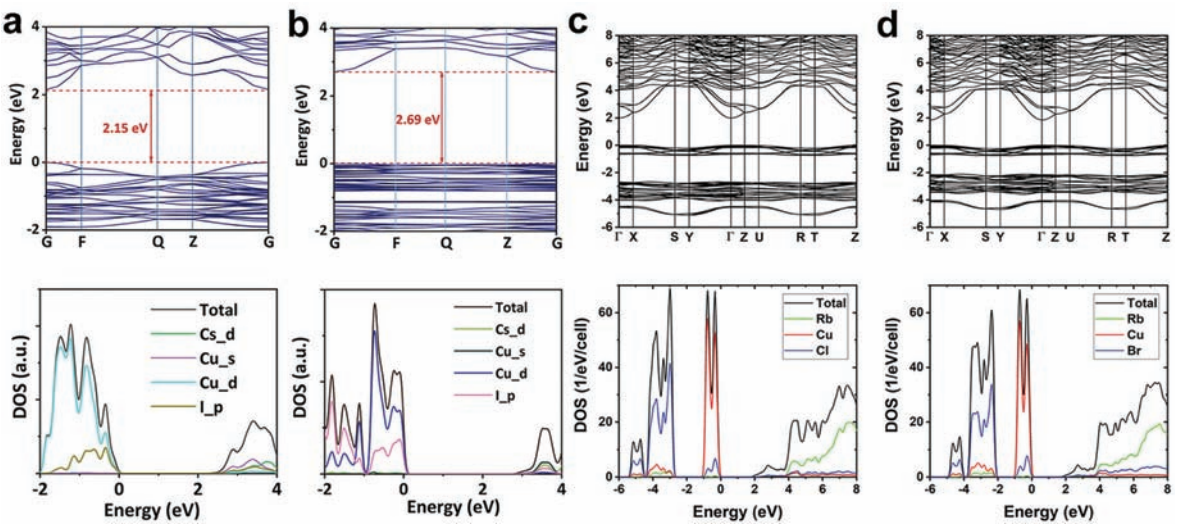

Fig. 5 Electronic band structure (top) and computed DOS (bottom) of Cu(I)-based metal halides. (a) 1D $CsCu_2I_3$, (b) 0D $Cs_3Cu_2I_5$. Reproduced with permission from ref. 41. Copyright 2019, Wiley-VCH. (c) 1D Ru_2CuCl_3 and (d) 1D Ru_2CuBr_3. Reproduced with permission from ref. 55. Copyright 2019, Wiley-VCH. Note that the band gap is underestimated by the PBE calculations.

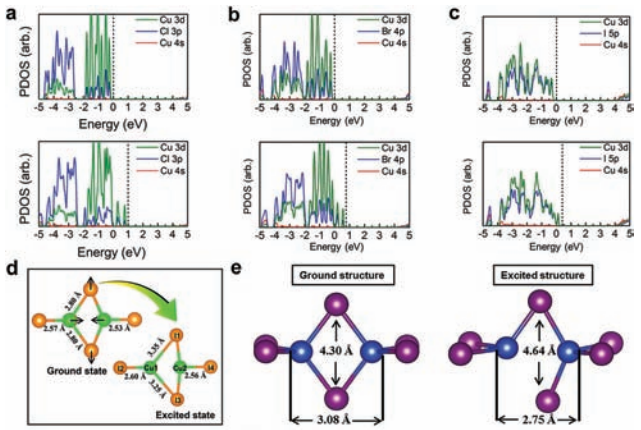

Fig. 6 Changes in the electronic structure of Cu(I)-based metal halides upon photoexcitation. Projected DOS for pristine (top) and distorted (bottom) structures of (a) $Cs_3Cu_2Cl_5$, (b) $Cs_3Cu_2Br_5$ and (c) $Cs_3Cu_2I_5$. Reproduced with permission from ref. 43. Copyright 2020, American Chemical Society. Geometric ground state and excited state structures of (d) the $[Cu_2I_5]^{3-}$ cluster. Reproduced with permission from ref. 45. Copyright 2020, American Chemical Society. (e) $CsCu_2I_3$. Reproduced with permission from ref. 65. Copyright 2020, American Chemical Society.

characteristic of the self-trapped exciton (STE) emission for Cu (I)-based halides.[44–46,65]

4.2 Optical properties

4.2.1 Composition-related PL emission. Similar to that of lead-based halides, the emission peak of Cu(I)-based halides could also be conveniently regulated by controlling the reaction temperature and stoichiometry of the precursor halide compositions.[41–44,55,62,69] The PL spectra of the as-prepared 0D $Cs_3Cu_2X_5$ (X = Cl, Br, and I) NCs, as depicted in Fig. 7a, show an abnormal blueshift from the green to blue region when halogen goes from Cl to I. Such a blueshift is attributed to the synergetic combination of the significant change in the bandgap associated with the structural deformation and large excitonic effect.[43] Both $Cs_3Cu_2Cl_5$ and $Cs_3Cu_2I_5$ exhibit quite a long lifetime, reaching 135.97 and 1.56 μs, respectively (Fig. 7b).[44]

Apart from modulation of the precursor halide compositions, it was found that adjusting the reaction temperature for synthesis from 110 to 160 °C allowed the emission peak to be tuned from 444 to 561 nm, which is due to the phase transition of 0D $Cs_3Cu_2I_5$ to 1D $CsCu_2I_3$.[42] In contrast, the emission peak of single halides $CsCu_2X_3$ (X = Cl, Br, I) shows a continuous redshift, while the mixed halides $CsCu_2Cl_{1.5}Br_{1.5}$ and $CsCu_2Br_{1.5}I_{1.5}$ do not follow a linear trend (Fig. 7c–e).[69] Particularly, the PL lifetime of $CsCu_2X_3$ shows the opposite

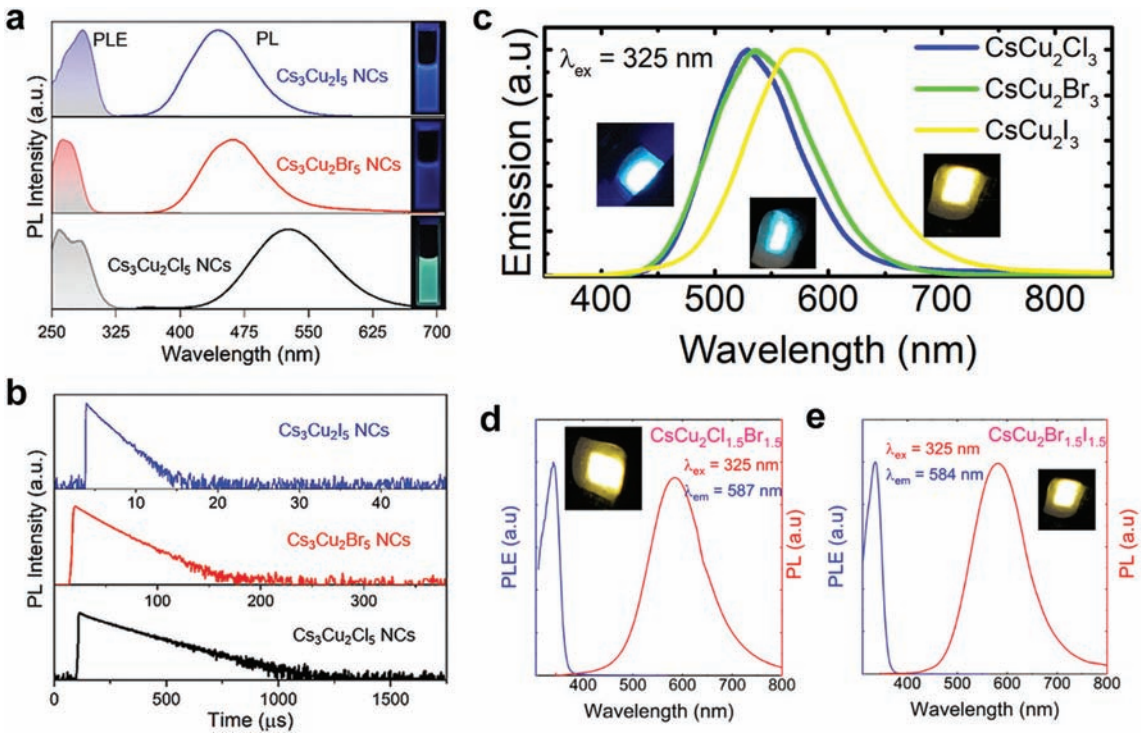

Fig. 7 Composition-related PL emission of Cu(I)-based metal halides. (a) PL excitation and emission spectra of colloidal $Cs_3Cu_2X_5$ NC solutions in hexane. Right insets show the photographs of $Cs_3Cu_2X_5$ NC solutions under 254 nm excitation. (b) Time-resolved PL decay spectra of $Cs_3Cu_2X_5$ NC solutions. Reproduced with permission from ref. 44. Copyright 2020, Wiley-VCH. (c) PL spectra of $CsCu_2X_3$ under 325 nm excitation. PL excitation (blue) and emission (red) spectra of (d) $CsCu_2Cl_{1.5}Br_{1.5}$ and (e) $CsCu_2Br_{1.5}I_{1.5}$. Reproduced with permission from ref. 69. Copyright 2019, American Chemical Society.

change trend to that of $Cs_3Cu_2X_5$, increasing from 13.8 ns for $CsCu_2Cl_3$ to 62 ns for $CsCu_2I_3$. The substitution of metal Rb ions for Cs ions results in the formation of strong violet emission halides Rb_2CuX_3 (X = Br and Cl), which is an additional strategy for modulating PL.[55,56] Furthermore, Kentsch *et al.*[72] provided direct experimental evidence of the exciton self-trapping mechanism through the femtosecond UV-vis transient absorption experiments of $CsCu_2I_3$ thin films.

4.2.2 Temperature-dependent PL emission. The thermal quenching phenomenon inevitably occurs in various luminescent materials, and the PL intensity gradually decreases with increasing temperature.[73,74] Research on the temperature-dependent PL behavior of semiconductors is very useful for us to understand the photophysical processes of materials. To get further information about the emission mechanisms, the temperature-dependent PL properties of the $Cs_3Cu_2I_5$ NCs and $CsCu_2I_3$ thin film were explored.[45,65] It was observed that the PL intensity of $Cs_3Cu_2I_5$ NCs continually decreased as the temperature was increased from 10 K to 300 K, whereas the emission peak positions remained almost unchanged (Fig. 8a). However, as shown in Fig. 8b, yellow-emitting $CsCu_2I_3$ exhibits a continuous blue-shift trend with increasing temperature.[65] A similar blue-shift was also observed in almost all the $CsCu_2X_3$ compounds by Roccanova and his colleagues (Fig. 8c).[69] Such an abnormal blue-shift phenomenon could be attributed to the high lattice distortion and the electron–phonon renormalization.[65,69] In addition, owing to the emission intensity associated with Cu^+ ions that is more sensitive to temperature than that associated with Mn^{2+} ions, the emission color of Mn(II)-doped $Cs_3Cu_2I_5$ microparticles changes from cyan to green when increasing the temperature from 298 to 498 K.[70] Furthermore, Lian *et al.*[43] investigated the time-resolved PL decay lifetimes of $Cs_3Cu_2Cl_5$ at various temperatures (Fig. 8d). They found that the change rate of lifetime with respect to temperature was as high as 2.7 μs $°C^{-1}$. In fact, through the measurements of temperature-dependent PL spectra of semiconductor materials, their corresponding photophysical parameters (such as exciton binding energy, optical phonon energy, exciton–phonon coupling constant, *etc.*) can be obtained, which is also vital for us to analyze the relevant mechanism.[40,45,48,52,65,69] However, further efforts could be focused on the temperature dependent transient PL spectra, which can reveal more physical chemistry processes in Cu(I)-based halides.

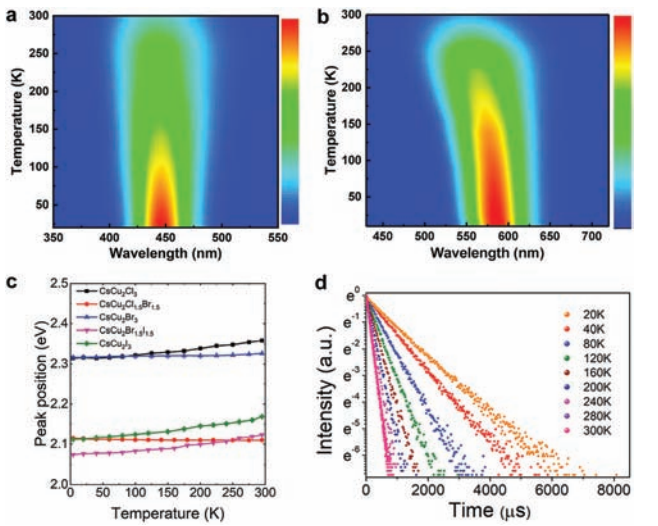

Fig. 8 Temperature-dependent PL emission of Cu(I)-based metal halides. Pseudo-color map of temperature-dependent PL spectra of (a) $Cs_3Cu_2I_5$ NCs. Reproduced with permission from ref. 45. Copyright 2020, American Chemical Society. (b) $CsCu_2I_3$ thin films. Reproduced with permission from ref. 65. Copyright 2020, American Chemical Society. (c) Thermal evolution of PL peak position of $CsCu_2X_3$. Reproduced with permission from ref. 69. Copyright 2019, American Chemical Society. (d) Time-resolved PL decay of $Cs_3Cu_2Cl_5$. Reproduced with permission from ref. 43. Copyright 2020, American Chemical Society.

4.2.3 Pressure-induced enhanced PL emission. Pressure-induced emission of low-dimensional metal halides has already been reported by Ma's group.[75] Most recently, as a unique mechanism to regulate the luminescence of metal halides, Li *et al.*[54] investigated the pressure-induced enhanced PL emission of 1D Cu(I)-based halide $CsCu_2I_3$. As shown in Fig. 9a–c, the emission color of the $CsCu_2I_3$ crystal gradually changes from yellow to green with the increase in pressure to 4.1 GPa. With continuous compression to 8.0 GPa, the emission intensity is significantly enhanced under ambient conditions, whereas further compression leads to quenching of emission intensity.[54] The major reason for this phenomenon is due to the large structural distortions from intra- and inter-tetrahedra, which has been proved through high-pressure angle-dispersive X-ray diffraction.[54] In short, the in-depth study of pressure-induced enhanced PL behavior of Cu(I)-based halides is essential for further understanding the structure–property relationships, which in turn depends on the effect of pressure on the lattice structure.

4.2.4 Polarization-dependent PL emission. Recently, semiconductor NWs, with a facile-engineered dimension and well-defined structural anisotropy, have demonstrated remarkable light polarization characteristics from various aspects of emission, absorption, and photoconductivity.[76] As stated in the crystal structure section, $CsCu_2I_3$ has a 1D anisotropic crystal structure, which makes it tend to grow into a 1D linear morphology.[48] Fig. 9d illustrates the variation in the PL intensity of 1D $CsCu_2I_3$ NWs with respect to the polarization angle.[49] The PL intensity shows the maximum value at an angle of 0° then decreases gradually with a change in the polarization angle and reaches the minimum at 90° polarization (Fig. 9e). In addition, the emission polarization ratio is calculated to be ~1.7 : 1, which results from the anisotropic crystal structure and morphology simultaneously.[49] The polarization-dependent PL properties of the Cu(I)-based $CsCu_2I_3$ NWs possess high potential for being applied in polarization-sensitive UV photodetectors.

4.3 Stability

The air-, photo- and thermal-stability issues of metal halides in an atmospheric environment and over a wide temperature

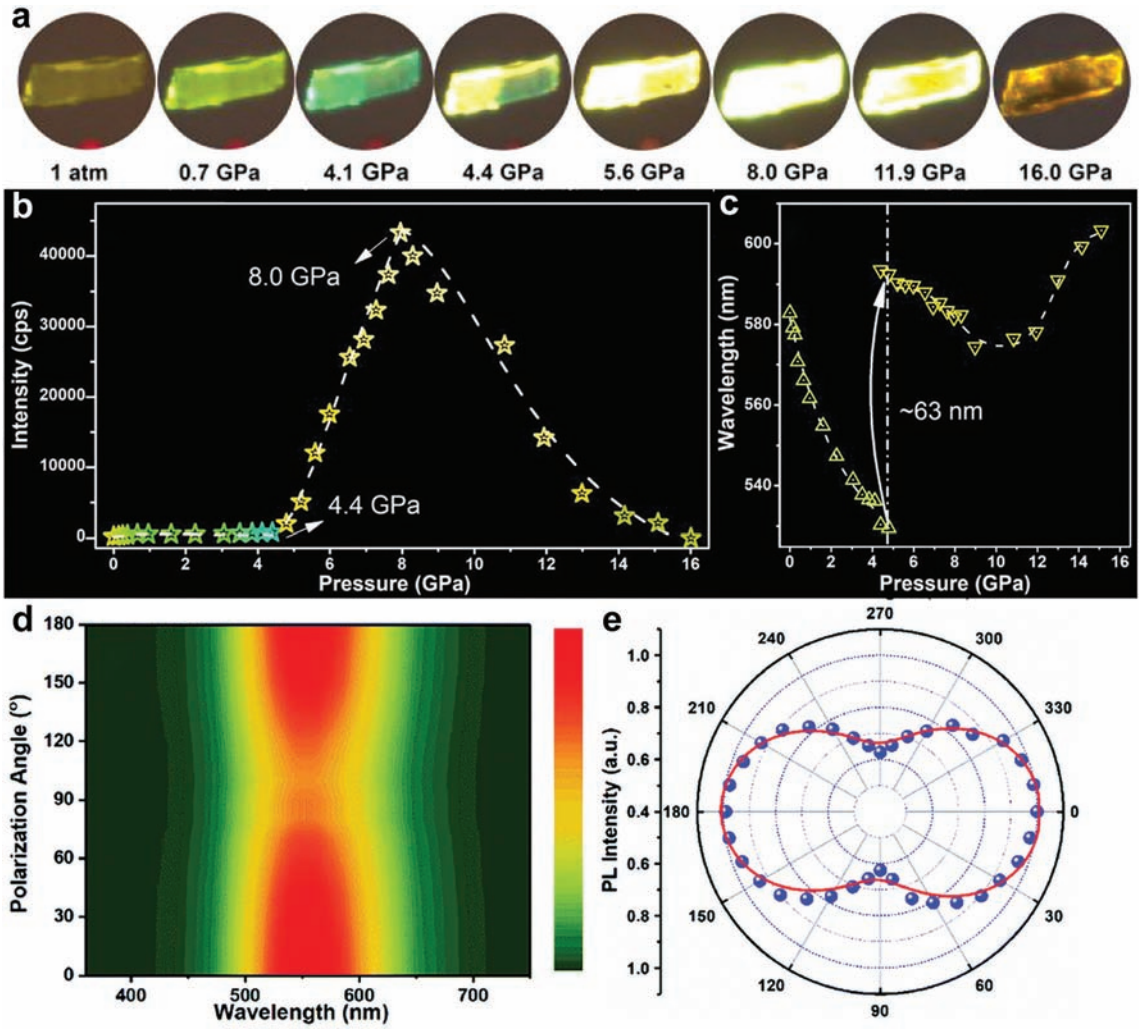

Fig. 9 Pressure-induced enhanced and polarization-dependent PL emission of Cu(I)-based metal halides. (a) PL micrographs of $CsCu_2I_3$ crystal under ambient conditions and compression up to 16.0 GPa. (b) Evolution of STE emission peak maximum intensity as a function of pressure. (c) Pressure-dependent shifts of PL peaks. Reproduced with permission from ref. 54. Copyright 2020, American Chemical Society. (d) PL spectra as a function of the incident light polarization. (e) Polarization-dependent PL intensity of 1D $CsCu_2I_3$ NWs. The data (blue dots) are fitted with a cosine function (red line). Reproduced with permission from ref. 49. Copyright 2020, the Royal Society of Chemistry.

range are essential for further long-term commercial implementation. However, due to the low exciton binding energy, traditional metal halides possess physical instability, resulting in easy diffusion and decomposition of ions into various dimensional phases.[29,33] In addition, these materials are chemically unstable and can easily react with water and oxygen molecules in the air environment, and the phase separation also occurs upon photoexcitation.[5,77] Fortunately, low-dimensional Cu(I)-based metal halides exhibit excellent stability, in which $CsCu_2X_3$ (X = Cl, Br, I) and $Cs_3Cu_2I_5$ both show good ambient air stability for more than two months.[40,41,69] However, as a result of the oxidation of Cu^+ to Cu^{2+}, $Cs_3Cu_2Cl_5$ with high PLQY exhibits poor air stability, whereas moisture-induced oxidation does not occur with copper iodide, resulting in favorable stability of $Cs_3Cu_2I_5$.[62] Furthermore, as for blue-emitting halide $Cs_3Cu_2I_5$ and yellow-emitting halide $CsCu_2I_3$, a tiny decay was generated after continuous UV light irradiation for a long time (*cf.* $Cs_3Cu_2I_5$: the attenuation is 2% after 8 h, $CsCu_2I_3$: 5% after 750 min).[48,61] The inherent excellent stability of Cu(I)-based halides shows them to possess broad prospects in optoelectronic applications, which will be discussed in the next section.

5. Applications

5.1 LEDs

LEDs based on metal halides have attracted extensive research interest due to their potential applications in lighting and displays. Cu(I)-Based metal halide LEDs are emerging due to their nontoxicity and excellent stability.[40,45,65,69] Typically, these LEDs consist of a hole-providing and electron-blocking layer,

the emitting layer and an electron-providing and hole-blocking layer. The emitting film layer is usually fabricated either by spin-coating the NCs dispersion onto the substrate, or by adding dropwise the anti-solvent onto the substrate coated with stoichiometric CsI and CuI precursors, which has been discussed in the Synthesis section. Considering the inherent phase instability of Pb-based mixed halide yellow LEDs caused by halide separation under continuous operating bias, Ma's group for the first time fabricated highly stable yellow LEDs based on all-inorganic Cu(I)-based halides $CsCu_2I_3$.[65] This device structure contains multiple layers as described below: ITO (anode), PEDOT:PSS (hole-injecting layer), poly-TPD (hole-transporting layer), $CsCu_2I_3$ thin films (emitting layer), TPBi (electron-transporting and hole-blocking layer), and LiF/Al (cathode), as shown in Fig. 10a and b. This as-designed LED has a relatively high turn-on voltage (~5.0 V) and a maximum luminance value of 47.5 cd m^{-2} at an applied bias voltage of 9.2 V (Fig. 10c).[65] In addition, they also investigated the EL spectra under various applied biases, the external quantum efficiency (EQE) and current efficiency, and half-lifetime (T_{50}) of the LEDs.

In terms of lifetimes, for all-inorganic metal halide LEDs, $Cs_3Cu_2I_5$ NCs were used by Wang *et al.*[45] to manufacture high-efficiency deep-blue LEDs with a half-lifetime above 100 h (Fig. 10d). This blue LED has a turn-on voltage (~4.5 V) and a maximum luminance (L_{max}) value of 262.6 cd m^{-2} at 7.5 V with the Commission Internationale de L'Eclairage (CIE) chromaticity diagram of (0.16, 0.07). The EQE of the $Cs_3Cu_2I_5$-based device was found to reach as high as ~1.12% at an applied bias voltage of 7.5 V (Fig. 10e) and is comparable with that of the best performing blue LEDs based on lead halides.[45] Additionally, they demonstrated that the reproducible and stable performances of the proposed device can serve as a reliable excitation source to convert the visible emission (Fig. 10f).[45] A detailed comparison of the parameters of these two Cu(I)-based LEDs is shown in Table 2.

5.2 Photodetectors

Ultraviolet (UV) photodetectors with high spectral selectivity have important applications in fluorescence detection, imaging, ultraviolet phototherapy and biomedical sensing. Li *et al.*[61] successfully constructed the $Cs_3Cu_2I_5$/GaN heterojunc-

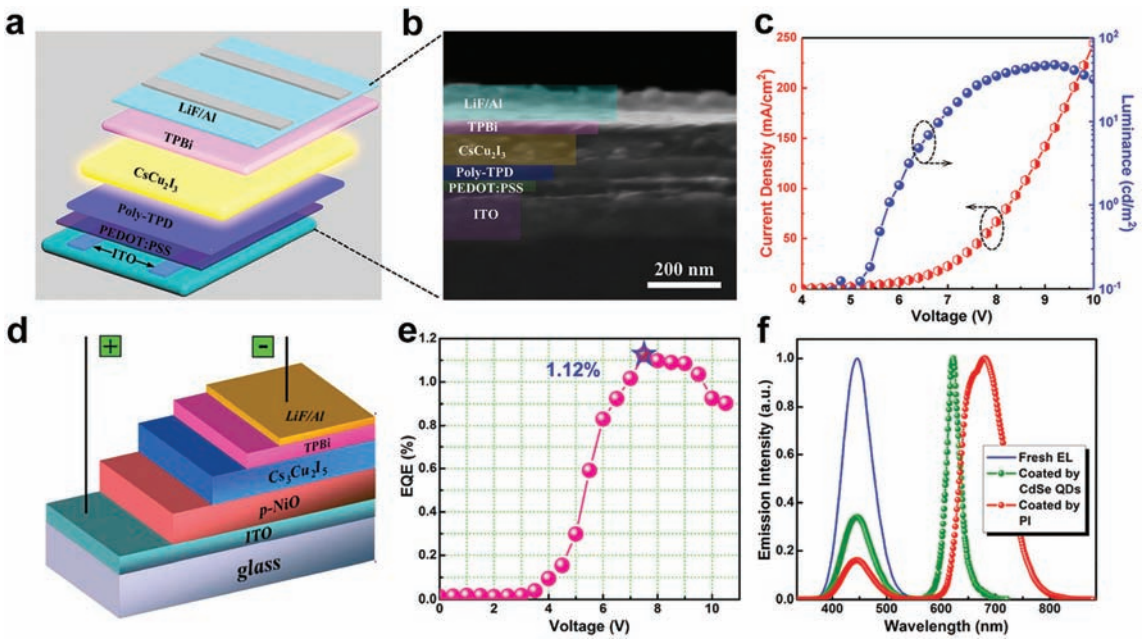

Fig. 10 LEDs based on ternary copper(I) halides. (a) Schematic illustration of the $CsCu_2I_3$ based LED with ITO/PEDOT heterostructure: PSS/poly-TPD/$CsCu_2I_3$/TPBi/LiF/Al. (b) Cross-sectional SEM image for the yellow LED structure. (c) Current density (red) and luminance (blue) as a function of voltage for the LEDs. Reproduced with permission from ref. 65. Copyright 2020, American Chemical Society. (d) Schematic structure of the $Cs_3Cu_2I_5$ NCs based LED. (e) Dependence of EQE of the $Cs_3Cu_2I_5$ NCs based device on bias voltage. (f) Comparison of the EL spectra from the pristine $Cs_3Cu_2I_5$ NCs based device as well as CdSe QD- and PI-coated devices. Reproduced with permission from ref. 45. Copyright 2020, American Chemical Society.

Table 2 Comparison of the main parameters of Cu(I)-based LEDs

Emission material	Color	EL λ_{max} (nm)	CIE	L_{max} (cd m^{-2})	EQE_{max} (%)	T_{50} (h)	Ref.
$CsCu_2I_3$	Yellow	550	(0.43, 0.52)	47.5	0.17	5.2	65
$Cs_3Cu_2I_5$	Blue	445	(0.16, 0.07)	262.6	1.12	108	45

tion and further fabricated spectrum-selective UV photodetectors by using the charge collection narrowing concept (Fig. 11a). The response window of the device is 300–370 nm by adjusting the thickness of the $Cs_3Cu_2I_5$ film, in which the response range shows a decreasing trend with an increase in the thickness (Fig. 11b). At zero bias, the device has a responsivity up to 0.28 A W^{-1}, a specific detection rate of 1.4×10^{12} Jones, a maximum current on/off ratio of 1.2×10^5, a response speed of 95/130 μs and the ability to respond to ultrafast optical signals (Fig. 11c–f), which are comparable to those of many previously reported lead halide photodetectors.[61] More importantly, metal halide $Cs_3Cu_2I_5$ has excellent UV resistance, ambient water/oxygen, and thermal stability, thereby the unencapsulated device can work continuously in air at a high temperature (373 K). Furthermore, after being enclosed in the open air for one month, the light detection capability of the device can still be maintained, demonstrating the unique advantages as a stable and efficient light detection material.[61] Subsequently, they applied optically anisotropic 1D $CsCu_2I_3$ NWs to manufacture polarization-sensitive and flexible UV photodetectors with a high photocurrent anisotropy ratio of ~3.16 (Fig. 11g and h).[49] The on/off ratio, response speed, photoresponsivity and specific detectivity reached 2.6×10^3, 6.94/214 μs, 32.3 A W^{-1} and 1.89×10^{12} Jones, respectively. The as-designed device also showed superior bending durability and working stability which could stand under wide angle (0°–160°) and increased bending cycles (~1000 times) (Fig. 11i).[49] In addition, Zhang *et al.*[60] also reported a sensitive deep UV photodetector based on the all-inorganic $Cs_3Cu_2I_5$ film derived by a solution method, which fully confirms great potential for future UV optoelectronic devices and systems. Very recently, facet-dependent photoresponse was observed for the $CsCu_2I_3$ single crystal by Li's group.[78] They proved that the on–off ratio of the {010} crystal plane is higher than that of the {110} crystal plane, which is attributed to the higher electron density of the {110} crystal plane, corresponding to higher dark

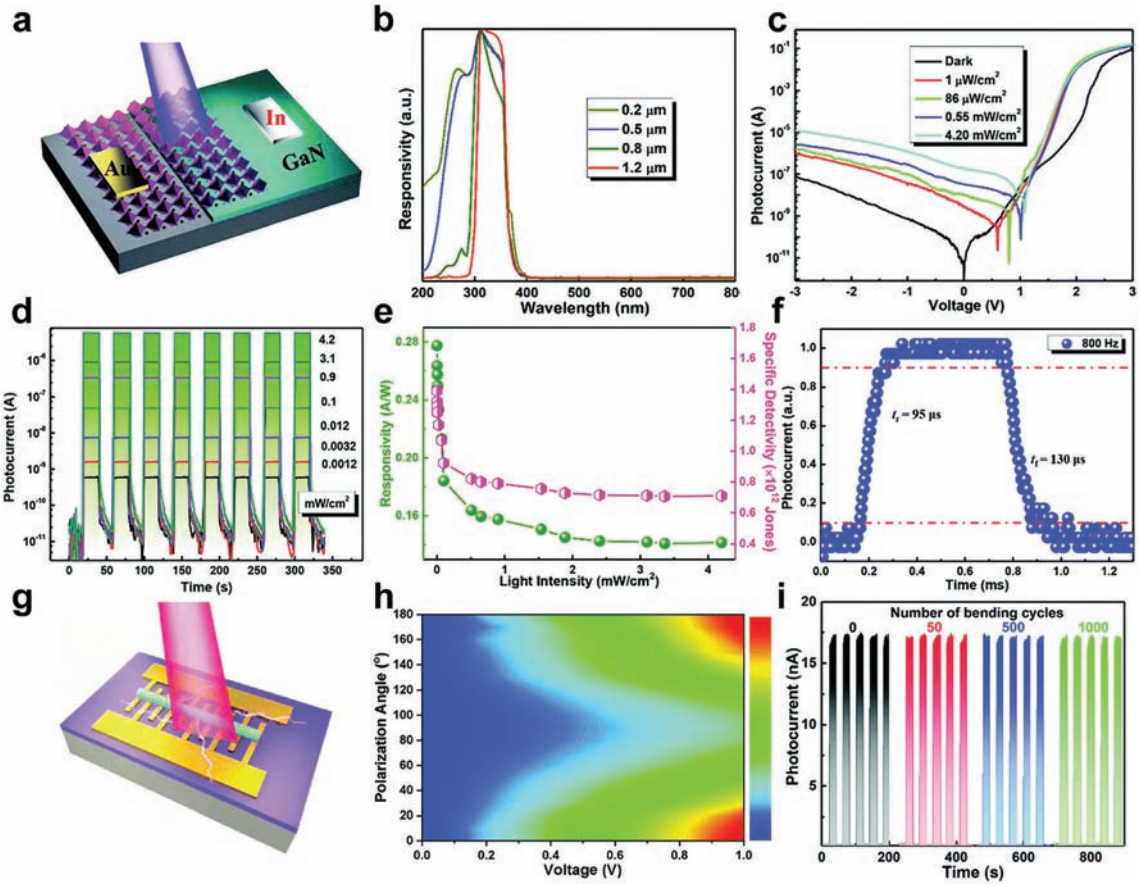

Fig. 11 Photodetectors based on ternary copper(I) halides. (a) Schematic illustration of the $Cs_3Cu_2I_5$/GaN heterojunction device. The $Cs_3Cu_2I_5$/GaN based photodetector: (b) response spectra with different absorber thicknesses, (c) *I*–*V* curves in the dark and under different light irradiation intensities (320 nm), (d) photocurrent response under 320 nm light excitation with varying intensity at zero bias, (e) responsivity and specific detectivity at various light intensities, (f) rising and falling edges for estimating the rise time (t_r) and fall time (t_f). Reproduced with permission form ref. 61. Copyright 2020, the Royal Society of Chemistry. (g) Schematic illustration of the photodetector based on an individual $CsCu_2I_3$ NW. The $CsCu_2I_3$ NW based photodetector: (h) anisotropic response in photocurrent under 325 nm excitation, (i) *I*–*t* curves under different bending cycles. Reproduced with permission from ref. 49. Copyright 2020, the Royal Society of Chemistry.

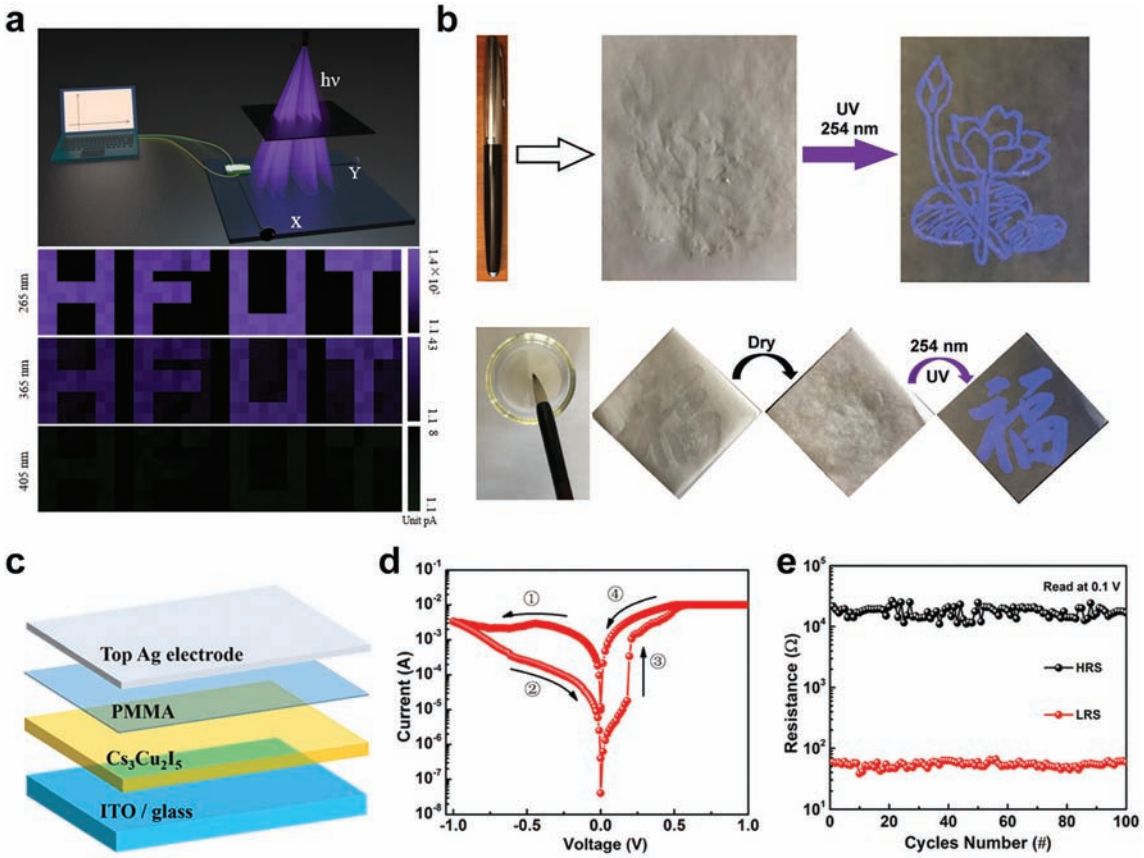

Fig. 12 Other applications based on ternary copper(I) halides. (a) Schematic illustration of the setup for recording deep UV image (top) and the image-sensing profile of HFUT under 265, 365, and 405 nm light excitation (bottom). Reproduced with permission from ref. 60. Copyright 2019, American Chemical Society. (b) Illustration of $Cs_3Cu_2I_5$ precursor solution as a fluorescent ink. Reproduced with permission from ref. 59. Copyright 2020, Wiley-VCH. (c) Schematic diagram, (d) typical RS *I*–*V* curves, and (e) endurance read at 0.1 V of Ag/PMMA/$Cs_3Cu_2I_5$/ITO memristor. Reproduced with permission from ref. 80. Copyright 2020, American Chemical Society.

current. Overall, all-inorganic Cu(I)-based metal halides are promising candidates for low-cost, high-performance UV photodetectors.

5.3 Other applications

The possibilities of Cu(I)-based metal halides have also been explored in some other applications, such as image sensors,[60,61] fluorescent inks,[59] X-ray scintillators,[56,57,79] memristors and neuromorphic computing applications.[80] Image sensing is part of the potential optoelectronic applications. As described in Fig. 12a, the current signals from the heterojunction device prepared using $Cs_3Cu_2I_5$ halides and the corresponding position coordinates of the photo-mask were recorded in real time. Obviously, the purple and light purple images under 265 and 365 nm illumination can be readily formed, while no image can be seen at 405 nm, suggesting that Cu(I)-based halide thin film devices are reliable for UV light imaging function applications.[60] Moreover, inspired by evaporation crystallization, Zhang *et al.*[59] used precursor solution as an ink to prove the feasibility of $Cs_3Cu_2I_5$ for anti-counterfeiting and encryption applications. The written graphics showed colorless under sunlight, but became blue under UV light (Fig. 12b). Additionally, considering excellent luminescence performance and negligible self-absorption, Cu(I)-based metal halides exhibit a good scintillation response to X-ray signals, showing a large scintillation response of Rb_2CuCl_3 with a linear range from 48.6 nGy_{air} s^{-1} to 15.7 μGy_{air} s^{-1} and an appreciable light yield of 79 279 ($Cs_3Cu_2I_5$), 16 600 (Rb_2CuCl_3) and 91 056 (Rb_2CuBr_3) photons per meV, respectively.[56,57,79] Furthermore, the first attempt of 0D $Cs_3Cu_2I_5$ in the field of memristors and neuromorphic computing applications was also investigated very recently. The memristors based on 0D $Cs_3Cu_2I_5$ halide films were fabricated in a device structure of Ag/PMMA/$Cs_3Cu_2I_5$/ITO, exhibiting bipolar resistive switching (RS) with low operating voltage ($\leq \pm 1$ V), large on/off ratio (10^2), stable endurance (100 cycles), and long retention time ($>10^4$ s) (Fig. 12c–e).[80]

6. Conclusions and perspectives

Herein, the recent progress on all-inorganic Cu(I)-based ternary metal halides has been presented. We reviewed the synthesis strategy, crystal structure, stability, various properties

and related applications of all-inorganic Cu(I)-based ternary metal halides. Although the research on Cu(I)-based trihalide family has made impressive progress and major achievements, there are still plenty of new opportunities and challenges to be addressed in the future. The applications of low-dimensional Cu(I)-based metal halides have not been fully exploited, while the main objective of the current research is still to develop controllable synthesis strategies, characterize the structure and optical properties, as well as have a basic understanding of their structure–property relationships. Nevertheless, their unique photophysical properties are still of great significance for various potential applications, including LEDs, UV photodetectors, image sensing, scintillators, memristors, *etc*. Considering the fact that the nonlinear optical and chiral properties of traditional all-inorganic Pb-based metal halides have been widely investigated,[81–83] it is expected that the Cu(I)-based ternary metal halides can also be used in these fields. More interestingly, the broadband transparent window of the latter may enable them to exhibit efficient multiphoton absorption from visible to near infrared wavelength ranges. The fabrication of chiral Cu(I)-based ternary metal halides may also be a topic worth to be further studied, due to their potential applications in second harmonic generation and spintronics. In addition, nontoxicity and good stability under ambient conditions of Cu(I)-based ternary metal halides can provide additional advantages in future applications of environment-friendly optoelectronic devices. Furthermore, Manna *et al.*[84] reported Cu(I)-related metal halide $Cs_3Cu_4In_2Cl_{13}$ NCs with an unusual perovskite-like structure. In this structure, Cu(I) ions do not occupy the octahedral site, but form $[Cu_4Cl]^{3+}$ clusters with Cl ions, occupying 25% of the A sites and adopting tetrahedral coordination. They demonstrated that small inorganic cluster cations can occupy the A sites in the perovskite-like structures, which provides novel ideas for the design of Cu(I)-based metal halide materials.

Despite the latest progress in the synthesis of copper halides, highly effective synthesis of crystals with precise shape and size control compared to that of conventional lead halide semiconductors is still urgently needed to be explored. Even though Cu(I)-based ternary metal halides have demonstrated remarkable optical properties and long-term stability, they do not have a wider tunable spectrum compared to traditional Pb-based halides. Although component control strategies and physical mixing methods have been used to broaden their emission spectrum, the expansion of the red emission region remains to be unresolved, which may limit their wider applications. In addition, green-emitting $Cs_3Cu_2Cl_5$ NCs with near-unity PLQY are questioned for the lack of stability. Therefore, enhancing the stability of some certain Cu(I)-based ternary metal halides and maintaining high performance remain a challenge for commercial applications. Overall, although the prospect of all-inorganic Cu(I)-based ternary metal halides seems to be bright and clear, additional research work is still needed to improve the performance and stability of these materials before they can be put into industrial applications.

Conflicts of interest

The authors declare that they have no conflict of interest.

Acknowledgements

We acknowledge the financial support by the Natural Science Foundation of Guangdong Province (2019A1515012094), the Project of the Department of Education of Guangdong Province (2018KTSCX19) and the Shenzhen Basic Research Project of Science and Technology (JCYJ20190808121211510).

References

1 W. Xiang and W. Tress, *Adv. Mater.*, 2019, **31**, 1902851.
2 Y. Wu, X. Li and H. Zeng, *ACS Energy Lett.*, 2019, **4**, 673–681.
3 A. Dutta, R. K. Behera, P. Pal, S. Baitalik and N. Pradhan, *Angew. Chem.*, 2019, **131**, 5608–5612.
4 Z. Gu, Z. Zhou, Z. Huang, K. Wang, Z. Cai, X. Hu, L. Li, M. Li, Y. S. Zhao and Y. Song, *Adv. Mater.*, 2020, **32**, 1908006.
5 L. Protesescu, S. Yakunin, M. I. Bodnarchuk, F. Krieg, R. Caputo, C. H. Hendon, R. X. Yang, A. Walsh and M. V. Kovalenko, *Nano Lett.*, 2015, **15**, 3692–3696.
6 T. Moot, A. R. Marshall, L. M. Wheeler, S. N. Habisreutinger, T. H. Schloemer, C. C. Boyd, D. R. Dikova, G. F. Pach, A. Hazarika and M. D. McGehee, *Adv. Energy Mater.*, 2020, **10**, 1903365.
7 S. C. Liu, Z. Li, Y. Yang, X. Wang, Y. X. Chen, D. J. Xue and J. S. Hu, *J. Am. Chem. Soc.*, 2019, **141**, 18075–18082.
8 W. Xiang, Z. Wang, D. J. Kubicki, X. Wang, W. Tress, J. Luo, J. Zhang, A. Hofstetter, L. Zhang and L. Emsley, *Nat. Commun.*, 2019, **10**, 1–8.
9 H. Zhang, X. Fu, Y. Tang, H. Wang, C. Zhang, W. Y. William, X. Wang, Y. Zhang and M. Xiao, *Nat. Commun.*, 2019, **10**, 1–8.
10 M. Lu, Y. Zhang, S. Wang, J. Guo, W. W. Yu and A. L. Rogach, *Adv. Funct. Mater.*, 2019, **29**, 1902008.
11 H. Ding, W. Liu, Y. Zheng, C. Li, H. Jiang and X. Wang, *J. Mater. Chem. C*, 2019, **7**, 1690–1695.
12 H. Wang, X. Zhang, Q. Wu, F. Cao, D. Yang, Y. Shang, Z. Ning, W. Zhang, W. Zheng and Y. Yan, *Nat. Commun.*, 2019, **10**, 1–10.
13 S. Thapa, G. C. Adhikari, H. Zhu, A. Grigoriev and P. Zhu, *Sci. Rep.*, 2019, **9**, 1–10.
14 G. C. Adhikari, S. Thapa, H. Zhu and P. Zhu, *Adv. Opt. Mater.*, 2019, **7**, 1900916.
15 M. Gong, R. Sakidja, R. Goul, D. Ewing, M. Casper, A. Stramel, A. Elliot and J. Z. Wu, *ACS Nano*, 2019, **13**, 1772–1783.
16 R. Liu, H. Zhou, Z. Song, X. Yang, D. Wu, Z. Song, H. Wang and Y. Yan, *Nanoscale*, 2019, **11**, 9302–9309.

17 X. Huang, Q. Guo, S. Kang, T. Ouyang, Q. Chen, X. Liu, Z. Xia, Z. Yang, Q. Zhang and J. Qiu, *ACS Nano*, 2020, **14**, 3150–3158.

18 Y. Zhang, H. Zhu, J. Zheng, G. Chai, Z. Song, Y. Chen, Y. Liu, S. He, Y. Shi and Y. Tang, *J. Phys. Chem. C*, 2019, **123**, 4502–4511.

19 J. S. Han, Q. V. Le, J. Choi, H. Kim, S. G. Kim, K. Hong, C. W. Moon, T. L. Kim, S. Y. Kim and H. W. Jang, *ACS Appl. Mater. Interfaces*, 2019, **11**, 8155–8163.

20 L. Wang, P. Chen, P. S. Kuttipillai, I. King, R. Staples, K. Sun and R. R. Lunt, *ACS Appl. Mater. Interfaces*, 2019, **11**, 32076–32083.

21 J. Chen, Z. Luo, Y. Fu, X. Wang, K. J. Czech, S. Shen, L. Guo, J. C. Wright, A. Pan and S. Jin, *ACS Energy Lett.*, 2019, **4**, 1045–1052.

22 A. B. Wong, Y. Bekenstein, J. Kang, C. S. Kley, D. Kim, N. A. Gibson, D. Zhang, Y. Yu, S. R. Leone and L. W. Wang, *Nano Lett.*, 2018, **18**, 2060–2066.

23 L. J. Chen, *RSC Adv.*, 2019, **9**, 33847–33847.

24 Y. Cao, Z. Zhang, L. Li, J. R. Zhang and J. J. Zhu, *Anal. Chem.*, 2019, **91**, 8607–8614.

25 S. E. Creutz, H. Liu, M. E. Kaiser, X. Li and D. R. Gamelin, *Chem. Mater.*, 2019, **31**, 4685–4697.

26 H. Lin, C. Zhou, Y. Tian, T. Siegrist and B. Ma, *ACS Energy Lett.*, 2017, **3**, 54–62.

27 C. Zhou, H. Lin, Q. He, L. Xu, M. Worku, M. Chaaban, S. Lee, X. Shi, M. H. Du and B. Ma, *Mater. Sci. Eng., R*, 2019, **137**, 38–65.

28 P. Chen, Y. Bai, M. Lyu, J. H. Yun, M. Hao and L. Wang, *Sol. RRL*, 2018, **2**, 1700186.

29 M. I. Saidaminov, J. Almutlaq, S. Sarmah, I. Dursun, A. A. Zhumekenov, R. Begum, J. Pan, N. Cho, O. F. Mohammed and O. M. Bakr, *ACS Energy Lett.*, 2016, **1**, 840–845.

30 G. R. Yettapu, D. Talukdar, S. Sarkar, A. Swarnkar, A. Nag, P. Ghosh and P. Mandal, *Nano Lett.*, 2016, **16**, 4838–4848.

31 J. Li, X. Yuan, P. Jing, J. Li, M. Wei, J. Hua, J. Zhao and L. Tian, *RSC Adv.*, 2016, **6**, 78311–78316.

32 J. H. Cha, J. H. Han, W. Yin, C. Park, Y. Park, T. K. Ahn, J. H. Cho and D. Y. Jung, *J. Phys. Chem. Lett.*, 2017, **8**, 565–570.

33 H. Yang, Y. Zhang, J. Pan, J. Yin, O. M. Bakr and O. F. Mohammed, *Chem. Mater.*, 2017, **29**, 8978–8982.

34 X. Lian, X. Wang, Y. Ling, E. Lochner, L. Tan, Y. Zhou, B. Ma, K. Hanson and H. Gao, *Adv. Funct. Mater.*, 2019, **29**, 1807345.

35 Y. Lin, Y. Bai, Y. Fang, Q. Wang, Y. Deng and J. Huang, *ACS Energy Lett.*, 2017, **2**, 1571–1572.

36 B. M. Benin, D. N. Dirin, V. Morad, M. Wörle, S. Yakunin, G. Rainò, O. Nazarenko, M. Fischer, I. Infante and M. V. Kovalenko, *Angew. Chem., Int. Ed.*, 2018, **57**, 11329–11333.

37 J. Song, L. Xu, J. Li, J. Xue, Y. Dong, X. Li and H. Zeng, *Adv. Mater.*, 2016, **28**, 4861–4869.

38 H. Tsai, W. Nie, J. C. Blancon, C. C. Stoumpos, R. Asadpour, B. Harutyunyan, A. J. Neukirch, R. Verduzco, J. J. Crochet and S. Tretiak, *Nature*, 2016, **536**, 312–316.

39 M. Yuan, L. N. Quan, R. Comin, G. Walters, R. Sabatini, O. Voznyy, S. Hoogland, Y. Zhao, E. M. Beauregard and P. Kanjanaboos, *Nat. Nanotechnol.*, 2016, **11**, 872–877.

40 T. Jun, K. Sim, S. Iimura, M. Sasase, H. Kamioka, J. Kim and H. Hosono, *Adv. Mater.*, 2018, **30**, 1804547.

41 P. Cheng, L. Sun, L. Feng, S. Yang, Y. Yang, D. Zheng, Y. Zhao, Y. Sang, R. Zhang, D. Wei, W. Deng and K. Han, *Angew. Chem., Int. Ed.*, 2019, **58**, 16087–16091.

42 P. Vashishtha, G. V. Nutan, B. E. Griffith, Y. Fang, D. Giovanni, M. Jagadeeswararao, T. C. Sum, N. Mathews, S. G. Mhaisalkar, J. V. Hanna and T. White, *Chem. Mater.*, 2019, **31**, 9003–9011.

43 L. Lian, M. Zheng, P. Zhang, Z. Zheng, K. Du, W. Lei, J. Gao, G. Niu, D. Zhang, T. Zhai, S. Jin, J. Tang, X. Zhang and J. Zhang, *Chem. Mater.*, 2020, **32**, 3462–3468.

44 Z. Luo, Q. Li, L. Zhang, X. Wu, L. Tan, C. Zou, Y. Liu and Z. Quan, *Small*, 2020, **16**, 1905226.

45 L. Wang, Z. Shi, Z. Ma, D. Yang, F. Zhang, X. Ji, M. Wang, X. Chen, G. Na, S. Chen, D. Wu, Y. Zhang, X. Li, L. Zhang and C. Shan, *Nano Lett.*, 2020, **20**, 3568–3576.

46 R. Zhang, X. Mao, D. Zheng, Y. Yang, S. Yang and K. Han, *Laser Photonics Rev.*, 2020, **14**, 2000027.

47 T. Zuo, X. He, P. Hu and H. Jiang, *ChemNanoMat*, 2019, **5**, 278–289.

48 R. Lin, Q. Guo, Q. Zhu, Y. Zhu, W. Zheng and F. Huang, *Adv. Mater.*, 2019, **31**, 1905079.

49 Y. Li, Z. Shi, L. Wang, Y. C. Chen, W. Liang, D. Wu, X. Li, Y. Zhang, C. X. Shan and X. Fang, *Mater. Horiz.*, 2020, **7**, 1613–1622.

50 S. Fang, Y. Wang, H. Li, F. Fang, K. Jiang, Z. Liu, H. Li and Y. Shi, *J. Mater. Chem. C*, 2020, **8**, 4895–4901.

51 M. I. Saidaminov, A. L. Abdelhady, B. Murali, E. Alarousu, V. M. Burlakov, W. Peng, I. Dursun, L. Wang, Y. He and G. Maculan, *Nat. Commun.*, 2015, **6**, 1–6.

52 T. Jun, T. Handa, K. Sim, S. Iimura, M. Sasase, J. Kim, Y. Kanemitsu and H. Hosono, *APL Mater.*, 2019, **7**, 111113.

53 Y. Dang, Y. Liu, Y. Sun, D. Yuan, X. Liu, W. Lu, G. Liu, H. Xia and X. Tao, *CrystEngComm*, 2015, **17**, 665–670.

54 Q. Li, Z. Chen, B. Yang, L. Tan, B. Xu, J. Han, Y. Zhao, J. Tang and Z. Quan, *J. Am. Chem. Soc.*, 2020, **142**, 1786–1791.

55 T. D. Creason, A. Yangui, R. Roccanova, A. Strom, M. H. Du and B. Saparov, *Adv. Opt. Mater.*, 2020, **8**, 1901338.

56 X. Zhao, G. Niu, J. Zhu, B. Yang, J. H. Yuan, S. Li, W. Gao, Q. Hu, L. Yin and K. H. Xue, *J. Phys. Chem. Lett.*, 2020, **11**, 1873–1880.

57 B. Yang, L. Yin, G. Niu, J. H. Yuan, K. H. Xue, Z. Tan, X. S. Miao, M. Niu, X. Du, H. Song, E. Lifshitz and J. Tang, *Adv. Mater.*, 2019, **31**, 1904711.

58 R. Babu, L. Giribabu and S. P. Singh, *Cryst. Growth Des.*, 2018, **18**, 2645–2664.

59 F. Zhang, Z. Zhao, B. Chen, H. Zheng, L. Huang, Y. Liu, Y. Wang and A. L. Rogach, *Adv. Opt. Mater.*, 2020, **8**, 1901723.

60 Z. X. Zhang, C. Li, Y. Lu, X. W. Tong, F. X. Liang, X. Y. Zhao, D. Wu, C. Xie and L. B. Luo, *J. Phys. Chem. Lett.*, 2019, **10**, 5343–5350.

61 Y. Li, Z. Shi, W. Liang, L. Wang, S. Li, F. Zhang, Z. Ma, Y. Wang, Y. Tian, D. Wu, X. Li, Y. Zhang, C. Shan and X. Fang, *Mater. Horiz.*, 2020, **7**, 530–540.
62 P. Sebastia-Luna, J. Navarro-Alapont, M. Sessolo, F. Palazon and H. J. Bolink, *Chem. Mater.*, 2019, **31**, 10205–10210.
63 M. Xiao, F. Huang, W. Huang, Y. Dkhissi, Y. Zhu, J. Etheridge, A. Gray-Weale, U. Bach, Y. B. Cheng and L. Spiccia, *Angew. Chem., Int. Ed.*, 2014, **53**, 9898–9903.
64 N. J. Jeon, J. H. Noh, Y. C. Kim, W. S. Yang, S. Ryu and S. I. Seok, *Nat. Mater.*, 2014, **13**, 897–903.
65 Z. Ma, Z. Shi, C. Qin, M. Cui, D. Yang, X. Wang, L. Wang, X. Ji, X. Chen, J. Sun, D. Wu, Y. Zhang, X. J. Li, L. Zhang and C. Shan, *ACS Nano*, 2020, **14**, 4475–4486.
66 F. Zeng, Y. Guo, W. Hu, Y. Tan, X. Zhang, J. Yang, Q. Lin, Y. Peng, X. Tang, Z. Liu, Z. Yao and J. Du, *J. Lumin.*, 2020, **223**, 117178.
67 P. Pal, S. Saha, A. Banik, A. Sarkar and K. Biswas, *Chem. – Eur. J.*, 2018, **24**, 1811–1815.
68 Z. Y. Zhu, Q. Q. Yang, L. F. Gao, L. Zhang, A. Y. Shi, C. L. Sun, Q. Wang and H. L. Zhang, *J. Phys. Chem. Lett.*, 2017, **8**, 1610–1614.
69 R. Roccanova, A. Yangui, G. Seo, T. D. Creason, Y. Wu, D. Y. Kim, M. H. Du and B. Saparov, *ACS Mater. Lett.*, 2019, **1**, 459–465.
70 P. Du, P. Cai, W. Li, L. Luo, Y. Hou and Z. Liu, *Microchim. Acta*, 2019, **186**, 730.
71 S. Hull and P. Berastegui, *J. Solid State Chem.*, 2004, **177**, 3156–3173.
72 R. Kentsch, M. Morgenroth, M. Scholz, K. Xu, J. Schmedt, A. der Gunne, T. Lenzer and K. Oum, *J. Phys. Chem. Lett.*, 2020, **11**, 4286–4291.
73 A. Shinde, R. Gahlaut and S. Mahamuni, *J. Phys. Chem. C*, 2017, **121**, 14872–14878.
74 S. M. Lee, C. J. Moon, H. Lim, Y. Lee, M. Y. Choi and J. Bang, *J. Phys. Chem. C*, 2017, **121**, 26054–26062.
75 Z. Ma, Z. Liu, S. Lu, L. Wang, X. Feng, D. Yang, K. Wang, G. Xiao, L. Zhang, S. A. T. Redfern and B. Zou, *Nat. Commun.*, 2018, **9**, 1–8.
76 Y. Gao, L. Zhao, Q. Shang, Y. Zhong, Z. Liu, J. Chen, Z. Zhang, J. Shi, W. Du, Y. Zhang, S. Chen, P. Gao, X. Liu, X. Wang and Q. Zhang, *Adv. Mater.*, 2018, **30**, 1801805.
77 T. C. Jellicoe, J. M. Richter, H. F. J. Glass, M. Tabachnyk, R. Brady, S. E. Dutton, A. Rao, R. H. Friend, C. Dan and N. C. Greenham, *J. Am. Chem. Soc.*, 2016, **138**, 2941–2944.
78 Z. Li, Z. Li, Z. Shi and X. Fang, *Adv. Funct. Mater.*, 2020, **30**, 2002634.
79 L. Lian, M. Zheng, W. Zhang, L. Yin, X. Du, P. Zhang, X. Zhang, J. Gao, D. Zhang, L. Gao, G. Niu, H. Song, R. Chen, X. Lan, J. Tang and J. Zhang, *Adv. Sci.*, 2020, **7**, 2000195.
80 F. Zeng, Y. Guo, W. Hu, Y. Tan, X. Zhang, J. Feng and X. Tang, *ACS Appl. Mater. Interfaces*, 2020, **12**, 23094–23101.
81 J. Xu, X. Li, J. Xiong, C. Yuan, S. Semin, T. Rasing and X. H. Bu, *Adv. Mater.*, 2020, **32**, 2070017.
82 G. Long, R. Sabatini, M. I. Saidaminov, G. Lakhwani, A. Rasmita, X. Liu, E. H. Sargent and W. Gao, *Nat. Rev. Mater.*, 2020, **5**, 423–439.
83 T. He, J. Li, X. Li, C. Ren, Y. Luo, F. Zhao, R. Chen, X. Lin and J. Zhang, *Appl. Phys. Lett.*, 2017, **111**, 151102.
84 R. Kaiukov, G. Almeida, S. Marras, Z. Dang, D. Baranov, U. Petralanda, I. Infante, E. Mugnaioli, A. Griesi, L. De Trizio, M. Gemmi and L. Manna, *Inorg. Chem.*, 2020, **59**, 548–554.